Angular velocity of rotating black holes - a new way to construct initial data for binary black holes

Shuanglin Huang^{1,2}‡, Xuefeng Feng^{3,4}§ Yun-Kau Lau⁵||

¹Beijing Institute of Mathematical Sciences and Applications, Yanqihu, Huairou District, Beijing, 101408, China

²Yau Mathematical Sciences Center, Tsinghua University, Beijing, 100084, China ³Fudan Center for Mathematics and Interdisciplinary Study, Fudan University, Shanghai, 200433, China

 $^4{\rm Shanghai}$ Institute for Mathematics and Interdisciplinary Sciences (SIMIS), Shanghai, 200433, China

⁵Institute of Applied Mathematics, Morningside Center of Mathematics, Academy of Mathematics and System Science, Chinese Academy of Sciences, 55, Zhongguancun Donglu, Beijing, 100190, China

Abstract. Motivated by a geometric understanding of the angular velocity of a Kerr black hole in terms of a quasi-conformal map that describes a 2d Beltrami fluid flow, a new way to construct initial data sets for binary rotating black holes by prescribing the angular velocities of the two black holes at their horizons is discussed. A set of elliptic equations with prescribed Dirichlet boundary conditions at the horizons and at spatial infinity is established for constructing the initial data. To explore the dynamics encoded in these initial data, we consider the conformally flat three-metric case and numerically evolve it using the BSSN code for two co-rotating and counterrotating black holes with angular velocities prescribed at the horizons. When the angular velocities are non-uniform and deviate from a constant value at the horizons, new gravitational waveforms are generated which display certain oscillatory pattern reminiscent of that of quasi-normal ringing in the inspiral phase before merger takes place.

[‡] Joint first author.

[§] Joint first author.

Corresponding author, email: lau@amss.ac.cn.

1. Introduction

The aim of the present work is to propose a new method to construct initial data sets for the vacuum Einstein field equations by prescribing the dynamics of rotation at the black hole boundary, motivated primarily by our recent effort to understand the geometry of angular velocity of the Kerr metric[1]. For a constant time slicing of the Kerr metric, the momentum constraint can be written as a Beltrami equation[2], which appears in the context of two-dimensional fluid flow. The Beltrami equation is a fundamental tool in the study of quasi-conformal mappings and complex analysis. Furthermore, it offers a powerful framework for describing specific structures in two-dimensional fluid dynamics. The classical Beltrami equation governs a complex-valued function f through the relation

 $\frac{\partial f}{\partial \bar{z}} = \mu(z) \frac{\partial f}{\partial z}, \qquad |\mu(z)| < 1,$

where the function μ , known as the Beltrami coefficient, encapsulates the degree of non-conformality. A potential function can then be constructed for the momentum constraint and identified as the angular velocity of the Kerr metric. Since the construction is local, this fluid dynamical picture may be generalized to multiple black holes, in particular to binary black holes. Within the context of binary black holes, boundary conditions are prescribed at the apparent horizons in accordance with the rotational dynamics of these black holes. This enables us to establish a link between the spacetime dynamics in the vicinity of the horizons and the gravitational waveform extracted near null infinity in the time evolution of the initial data sets. Hopefully it offers an avenue to explore the dynamics of gravity near the horizon in relation to the gravitational wave form and gravitational wave will become a probe of the near horizon dynamics of binary black holes. For black holes with non-uniform angular velocities, as we shall see, the inspiral phase of the waveforms exhibits certain new features not seen before. Details of the construction are presented in the ensuing sections.

The paper is structured as follows. In Section II, we briefly describe the geometric description of the angular velocity of a Kerr black hole in terms of a quasi-conformal map. In Section III, within the conformally flat context, we build up a framework for the initial data construction by prescribing the angular velocity of a black hole at the horizon. In Section IV, by means of numerical simulation, we try to understand the gravitational waveform generated by the newly constructed initial data, to be followed by some concluding remarks in section V.

2. Angular velocity of a rotating black hole and the Kerr metric

In this section, we provide a brief geometric description of the angular velocity in the Kerr metric in terms of the momentum constraint on a constant time slice. This will pave the way for constructing initial data in terms of the angular velocities of binary black holes in what follows.

Consider the Kerr metric in the Boyer-Lindquist coordinates (t, r, θ, ϕ) , given by

$$ds^{2} = -\left(1 - \frac{2Mr}{\Sigma}\right) dt^{2} - \frac{4aMr\sin^{2}\theta}{\Sigma} dt d\phi + \frac{\Sigma}{\Delta} dr^{2} + \Sigma d\theta^{2} + \frac{A}{\Sigma} \sin^{2}\theta d\phi^{2},$$
(1)

where $A = (r^2 + a^2)^2 - \Delta a^2 \sin^2 \theta$, $\Sigma = r^2 + a^2 \cos^2 \theta$ and $\Delta = r^2 - 2Mr + a^2$.

Let K_{ab} denote the extrinsic curvature of the constant time slice, where the maximal slicing condition K = 0 is satisfied. Consider the vector field

$$V_a = K_{ab}\eta^b \,, \tag{2}$$

where $\eta^a = X^{-1/2}\phi^a$ is the normalized axisymmetric Killing vector and X is the norm of the axisymmetric Killing vector field ϕ^a . Further define $v_a = XV_a$. It may be inferred from the momentum constraint equation and the axisymmetric structure of V_a that, in terms of the flat connection ∂_a on the two-plane orthogonal to ϕ_a , the following Hodge-like system is satisfied.

$$\partial^a v_a = 0 \,, \tag{3}$$

$$\partial_{[a}\lambda X^{-\frac{3}{2}}v_{b]} = 0, \tag{4}$$

where λ is the stationary Killing field for the constant time slicing. Equations (3) and (4) resemble the Beltrami flow for a compressible fluid in the two-plane orthogonal to ϕ_a . A quasi-conformal equation can be further developed from (3) and (4) as

$$(w \Omega_x)_x + (w \Omega_y)_y = 0,$$

$$(w \Psi_x)_x + (w \Psi_y)_y = 0.$$
(5)

 Ω may be identified as the angular velocity of a rotating black hole, originally defined in terms of the stationary and axisymmetric Killing field. Ψ may be regarded as a stream function conjugate to Ω .

3. Angular velocities of binary black holes as initial data

When expressed in Weyl coordinates, the initial data set for the Kerr metric described in the preceding section suggests a very natural generalization to the case of Brill waves for binary rotating black holes, where the angular velocities of the black holes are treated as part of the initial data. As a first step toward understanding the construction of these new initial data sets, we shall consider a simple setting: a conformally flat initial data slice. The Bowen-York data are then employed as a benchmark for comparison with our construction.

Consider the conformally flat three-metric

$$\gamma_{ij} dx^i dx^j = \psi^4 (d\rho^2 + dz^2 + \rho^2 d\phi^2),$$
 (6)

where the flat metric is given in terms of standard cylindrical coordinates. Let K_{ij} denote the extrinsic curvature of the slice, and impose the maximal-slicing condition

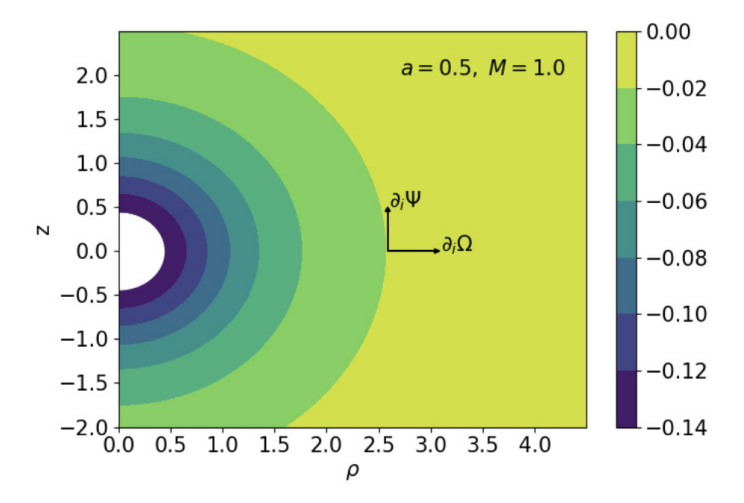


Figure 1: A Beltrami flow defined near the horizon by Ω and its conjugate stream function Ψ .

K = 0 on K_{ij} . Define tensor \bar{K}_{ij} as:

$$K_{ij} = \psi^{-2} \bar{K}_{ij} \,. \tag{7}$$

The constraint equations are then given by

$$\bar{D}^2 \psi + \frac{1}{8} \bar{K}_{ij} \bar{K}^{ij} \psi^{-7} = 0, \qquad (8)$$

$$\bar{D}_i \bar{K}^{ij} = 0, \tag{9}$$

where \bar{D} is defined as the covariant derivative operator with respect to the flat metric.

Let \bar{K}_{ij}^{Ω} be \bar{K}_{ij} subject to the momentarily stationary slicing condition (or equivalently, the (t, ϕ) -symmetric condition), such that

$$\bar{K}_{ii}^{\Omega}h^{im}h^{jn} = 0, \quad \bar{K}_{ii}^{\Omega}\phi^{i}\phi^{j} = 0. \tag{10}$$

Here h_{ij} is the two-metric induced by restricting γ_{ij} to the (ρ, z) plane, and ϕ^i denotes the azimuthal Killing vector $(\partial/\partial\phi)^i$. $\bar{K}^{\Omega}_{\rho\phi}$ and $\bar{K}^{\Omega}_{z\phi}$ are the only two independent, non-zero components of \bar{K}^{Ω}_{ij} . Further define the vector field \bar{V}_a

$$\bar{V}_i = \bar{K}_{ij}^{\Omega} \bar{\eta}^j \,, \tag{11}$$

where

$$\bar{\eta}^i = \rho^{-1} \phi^i \,.$$

As in the case of the Kerr metric, the vector field \bar{V}_i may be expressed by the angular velocity potential Ω as,

$$\bar{V}_i = -\frac{1}{2}\rho\partial_i\Omega. \tag{12}$$

where we have chosen the lapse function to be $\alpha = \psi^6$. \bar{K}_{ij}^{Ω} can be constructed from Ω as:

$$\bar{K}_{ij}^{\Omega} = \bar{\eta}_{(i}\bar{V}_{j)} = -\frac{1}{2}\rho\bar{\eta}_{(i}\partial_{j)}\Omega. \tag{13}$$

Given Eq.(13), the Hamiltonian and momentum constraint equations can be expressed as elliptic equations for the conformal factor ψ and the potential Ω :

$$\bar{D}^2 \psi + \frac{1}{8} \bar{K}_{ij} \bar{K}^{ij} \psi^{-7} = 0, \qquad (14)$$

$$\partial^i(\rho^3\partial_i\Omega) = 0. (15)$$

As it stands, axisymmetry of (13) means that the initial data constructed can only describe head-on collision of two black holes. To incorporate inspiral in the data, linearity of the momentum constraint (9) enables us to supplement (15) by adopting the linear momentum part of the Bowen-York ansatz into the initial data set. Specifically, we set:

$$\bar{K}_{ij} = \bar{K}_{ij}^P + \bar{K}_{ij}^\Omega \,. \tag{16}$$

in which

$$\bar{K}_{ij}^{P} = \frac{3}{2r_A^2} \left[P_{Ai} n_{Aj} + P_{Aj} n_{Ai} - (\delta_{ij} - n_{Ai} n_{Aj}) P_A^k n_{Ak} \right], \tag{17}$$

$$\bar{K}_{ij}^{\Omega} = -\frac{1}{2}\rho\bar{\eta}_{(i}\partial_{j)}\Omega. \tag{18}$$

Here P_A^i are constant vectors, and $r_A = ||x^i - c_A^i||$ is the coordinate distance to the center of black hole located at $x^i = c_A^i$, and $n_A^i = (x^i - c_A^i)/r_A$. \bar{K}_P^{ij} is the linear momentum part of the Bowen-York solution [3], in which P_A^i can be loosely regarded as the linear momentum of each black hole.

The spin part of the Bowen-York solution, which is not adopted in our method, is

$$\bar{K}_{ij}^S = \frac{3}{r_A^3} (n_{Ai}\epsilon_{jkl} + n_{Aj}\epsilon_{ikl}) S_A^k n_A^l, \qquad (19)$$

where constant vector S_A^i can be associated with the spin of each black hole in the limit of infinite separation. \bar{K}_{ij}^S also satisfies condition (10), and therefore it corresponds to a special choice of Ω in our method. Without loss of generality, we assume one black hole Bowen-York data with angular momentum directed along the z axis, i.e.:

$$S^{i} = (0, J, 0), (20)$$

$$n^{i} = \frac{1}{(\rho^{2} + z^{2})^{\frac{1}{2}}} (\rho, z, 0).$$
 (21)

then the non-zero terms of \bar{K}_{ij}^S are:

$$\bar{K}_{\rho\phi}^{S} = \bar{K}_{\phi\rho}^{S} = \frac{3J\rho^{3}}{(\rho^{2} + z^{2})^{\frac{5}{2}}},$$
 (22)

$$\bar{K}_{z\phi}^S = \bar{K}_{\phi z}^S = \frac{3J\rho^2 z}{(\rho^2 + z^2)^{\frac{5}{2}}},$$
 (23)

It is straightforward to verify that this corresponds to

$$\Omega = \frac{J}{(\rho^2 + z^2)^{\frac{3}{2}}}.$$
 (24)

in \bar{K}_{ij}^{Ω} . This form of Ω corresponds to a particular spin distribution: it describes an axisymmetric rotation with total angular momentum J aligned along the z-axis, in which the angular velocity is uniform on spheres of constant $r = \sqrt{\rho^2 + z^2}$.

3.1. Boundary Conditions

The initial data are required to be asymptotically flat, and the outer boundary \mathcal{B}_{∞} is placed near infinity. The outer boundary condition for ψ is

$$\psi = 1 \quad \text{on } \mathcal{B}_{\infty} \,. \tag{25}$$

In the case of the Kerr metric, the angular velocity $\Omega = \mathcal{O}(r^{-3})$ when $r \to \infty$. It is reasonable to adopt a similar asymptotic behavior as the boundary condition for Ω at infinity in the binary case.

To specify boundary conditions for black hole initial data, we require the inner boundary to consist of marginally trapped surfaces. This leads to the following boundary condition:

$$\frac{\partial \psi}{\partial r} + \frac{\psi}{2r} + \frac{\bar{K}_{rr}}{4\psi^3} = 0. \tag{26}$$

Each trapped surface is chosen to be a coordinate two-sphere located at a constant radius r, where r is the radial coordinate centered on each black hole. It should be noted that this condition does not guarantee that the inner boundary coincides with the apparent horizon, which is defined as the outermost marginally trapped surface. However, in practice, once the initial data have been constructed, the apparent horizon can always be located as the outermost such surface.

In our numerical setup, we enforce the condition (26) as follows. We first prescribe Ω at the inner boundary according to the desired configuration, then solve for Ω and combine it with the specified \bar{K}_{ij}^P to construct \bar{K}_{ij} . Condition (26) is subsequently used as a boundary condition for solving the conformal factor ψ .

4. Waveform simulations

In order to understand the gravitational wave content of the newly constructed data, we present in this section the gravitational waveforms generated by the evolution of black hole initial data sets constructed using our method. To facilitate comparison with the Bowen-York initial data, we adjust the free parameters such that the Christoudoulou mass and spin of black holes are identical to those constructed using Bowen-York method.

4.1. Numerical settings

To construct the initial data, we developed an elliptic solver based on LORENE[4], a C++ library provides tools for solving PDEs using multi-domain spectral methods. We adopt the treatment in [5, 6], space is decomposed into various spherical-like shells, and the outermost shell is compactified using the variable u=1/r, which enables one to impose exact boundary conditions at infinity. For binary black holes, two sets of such domains are used. Each set is centered on one black hole, and the fields are decomposed into contributions defined on the two sets of domains.

The Einstein Toolkit [7, 8] is employed to simulate the evolution of black hole collisions and inspirals. For comparison, we also evolve standard Bowen-York initial data constructed using the TwoPunctures[9] thorn. Both sets of initial data are evolved using the McLachlan/ML_BSSN[10, 11] thorn, which implements the BSSN formulation[12, 13] of Einstein's equations, together with the Carpet[14] driver for adaptive mesh refinement. The apparent horizons of the black holes are located and tracked using the AHFinderDirect[15] thorn, and their quasi-local properties, such as mass and spin, are computed with the QuasiLocalMeasures[16] thorn. The gravitational wave signal is extracted via the WeylScal4 thorn.

4.2. Single spinning black hole

We first look at the single spinning black hole. Black hole spins are commonly characterized in terms of their dimensionless spin

$$\chi = \frac{S}{M_{\rm Chr}^2} \,. \tag{27}$$

Here S is taken to be non-negative and represents a suitable quasilocal spin, while M_{Chr} denotes the Christoudoulou mass [17] of the black hole, given by

$$M_{\rm Chr}^2 = M_{\rm irr}^2 + \frac{S^2}{4M_{\rm irr}^2} \,.$$
 (28)

The irreducible mass M_{irr} is defined in terms of the area of the black hole's apparent horizon:

$$M_{\rm irr} = \sqrt{\frac{A}{16\pi}}. (29)$$

Using a surface integral over the apparent horizon H, the Komar angular momentum can be calculated as follows[18, 19, 20]:

$$S = \frac{1}{8\pi} \oint_{H} \phi^{i} s^{j} K_{ij} dA = \frac{1}{8\pi} \oint_{H} (\psi^{4} \rho^{2})^{1/2} s^{i} V_{i} dA, \qquad (30)$$

where H denotes the black hole's apparent horizon, s^j is the outward-pointing unit normal to H within the t=const hypersurface, and ϕ^i is an azimuthal vector field tangent to H.

Fig. 2 shows the results for a single spinning black hole with inner boundary value of Ω prescribed as $\Omega|_{r=r_H} = \Omega_H \sin \theta$, where Ω_H is a constant parameter. In the plot, in addition to dimensionless spin χ , we also introduce two other dimensionless spin measures, ϵ and ζ , defined as

$$\epsilon = \frac{J_{ADM}}{E_{ADM}}, \quad \zeta = \frac{S}{2M_{\text{irr}}^2}. \tag{31}$$

 J_{ADM} and E_{ADM} denote ADM angular momentum and ADM energy, respectively. These three quantities χ , ϵ_J , and ζ are used to monitor whether a black hole becomes super-extremal, and it was observed that none of them reach or exceed unity as Ω_H/r_H^2 increases. These findings are in good agreement with the results reported in the literature [21, 22].

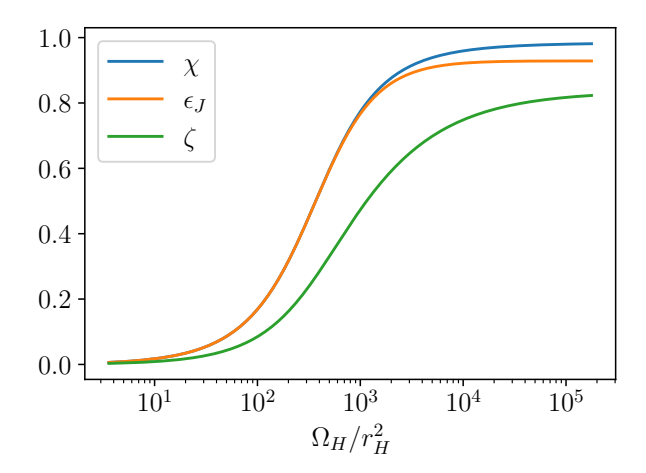


Figure 2: The three spin parameters χ , ϵ_J , and ζ for a single rotating black hole are plotted, where a value of zero denotes a non-spinning black hole and a value of one corresponds to an extremal case. As the value of Ω_H/r_H^2 increases, the parameters approach the following asymptotic values: $\chi_{\text{max}} = 0.984$, $\zeta_{\text{max}} = 0.823$, and $\epsilon_{J,\text{max}}(S/M_{\text{ADM}}^2) = 0.928$.

4.3. Constant Ω on the horizon and code calibration

For binary black holes, we first simulate the waveform with a constant value of Ω on the horizon. The waveform generated turns out to be nearly identical to that of the Bowen-York case as one would expect. This is consistent with the calculations in the previous section. This serves to calibrate our code so that, for the waveform generated by a more complicated choice of Ω which describes non-uniform angular velocity on the horizon in what follows, the deviation of waveform from that of Bowen-York is not due to numerical errors.

4.4. Head-on collisions

Next we set $\Omega|_{r=r_H} = \pm 82(3\cos^2\theta - 1)$, which is, up to a constant, proportional to the spherical harmonic component C_{20} (see the left panel in Fig. 3). The \pm sign corresponds to opposite spin directions. Certain oblateness in the angular velocity is injected in the rotating horizon. \bar{K}_P^{ij} is set to zero, so each black hole has no linear momentum initially. For the head-on collisions, no significant deviation from the Bowen-York waveform is observed, as shown in Fig. 4.

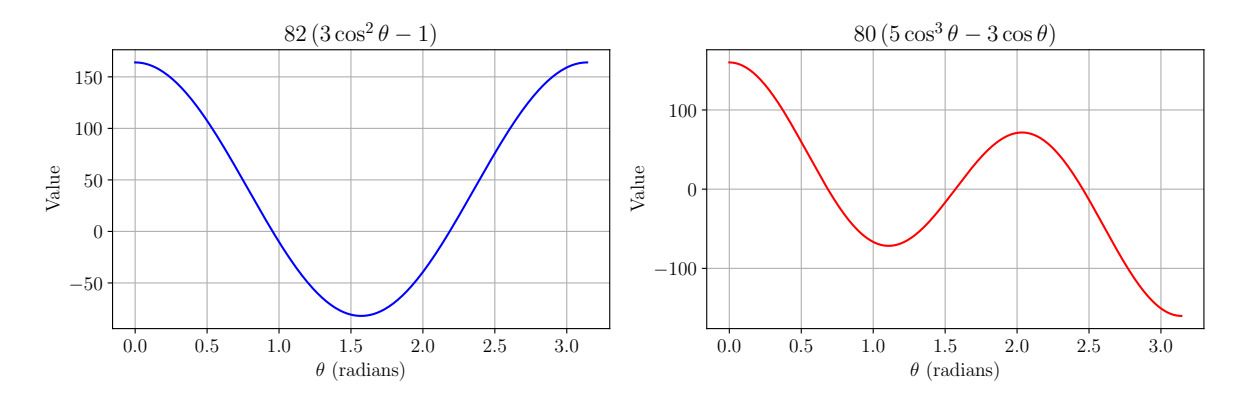


Figure 3: Angular velocity function $\Omega(\theta)$ evaluated at the horizon. The profile in the left panel corresponds to the models in Fig. 4, 5, and 7, while the one in the right panel is employed in Fig. 8.

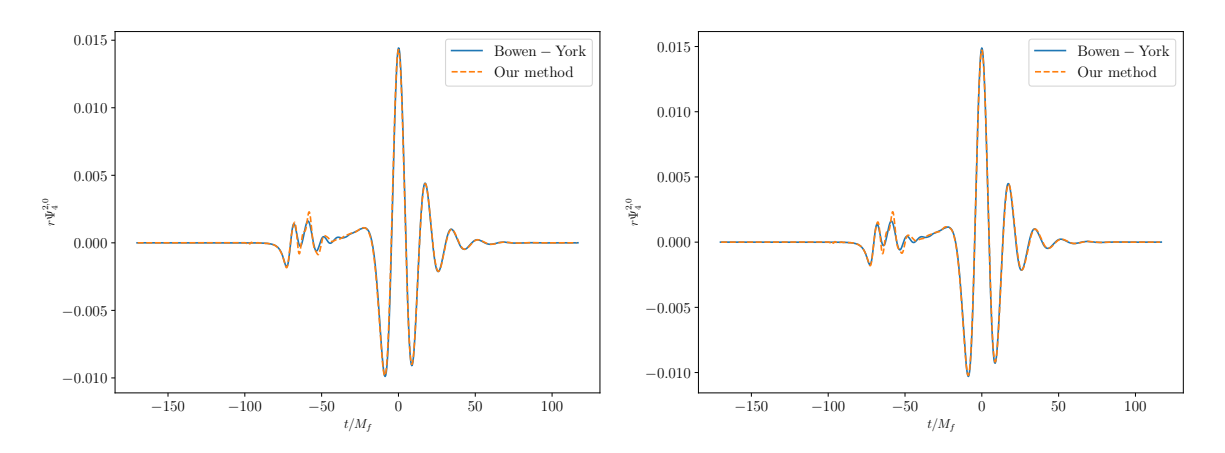


Figure 4: The gravitational radiation $r\Psi_4^{20}$ from the head-on collision of equalmass black holes produced by our initial data with the inner boundary condition for Ω prescribed as $\Omega|_{r=r_H}=\pm 82(3\cos^2\theta-1)$. Black holes have mass $M_1=M_2=$ 0.5493, and are initially placed at $z=\pm 6$. This is compared with Bowen-York black holes of the same masses and spins. Left: Both black holes have spins aligned along the +z axis. Right: The black holes have opposite spin directions, aligned along the +z and -z axes, respectively.

4.5. Black hole Inspiral

Next we activate \bar{K}_P^{ij} , and fine-tune the parameters such that the two black holes are initially in a nearly quasi-circular orbit. New features in the waveform begin to appear. As shown clearly in Fig. 5, and 7, the early-time waveform during the inspiral phase exhibits certain oscillatory pattern superposed on the overall inspiral waveform.

The early-time waveform resembles a ringdown-like signal, reminiscent of the findings in [23], which reported non-merging ringdown gravitational waves in simulations of hyperbolic black hole encounters. This connection supports the interpretation that the early ringdown-like features in our waveform are not gauge artifacts or residual junk

radiation, but physically meaningful emissions triggered by the initial configuration of the black holes.

To further confirm that these effects are physical rather than numerical artifacts, we perform a convergence test shown in Fig. 6. The left panel shows that the waveform converges as the resolution increases, with the phase exhibiting particularly strong agreement at higher resolutions. The right panel demonstrates that the Hamiltonian constraint violation decreases systematically with resolution, thereby confirming the consistency of the numerical simulation.

These results open the possibility that pre-merger QNM -like signatures, previously studied mostly in scattering or eccentric contexts, may also be present in quasi-circular binaries under certain initial conditions, though it is likely that the physical origins of the quasi-normal oscillatory pattern are different.

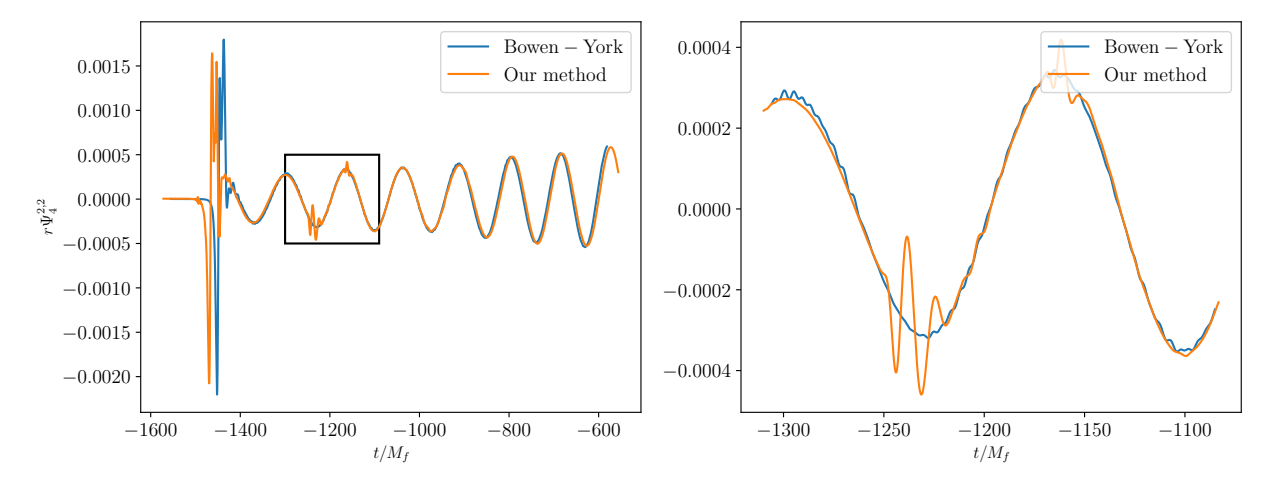


Figure 5: The gravitational radiation $r\Psi_4^{22}$ from the black hole inpiral of equalmass, with aligned spin direction. The inner boundary conditions for Ω is $\Omega|_{r=r_H} = 82(3\cos^2\theta - 1)$. The black holes have masses $M_1 = M_2 = 0.5511$, spins $S_1 = S_2 = (0.1312, 0, 0)$, and are initially placed at $x = \pm 6$. In the left panel, the enclosed box highlights an oscillatory pattern during the early phase of the merger. The right panel provides a zoomed-in view of this pattern.

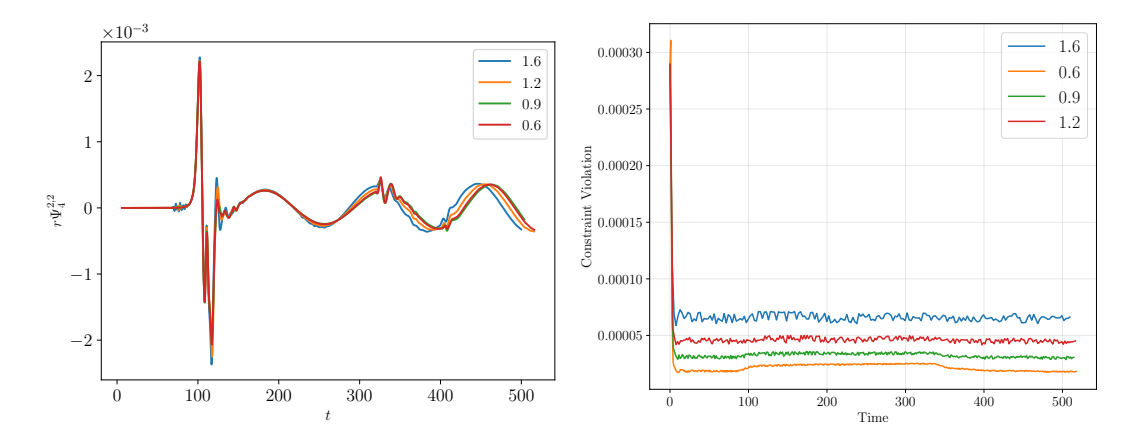


Figure 6: Convergence test for the simulation shown in Fig. 5. Left panel: Convergence of the waveform with increasing grid resolutions. Right panel: Systematic decrease of the Hamiltonian constraint violation with increasing grid resolution.

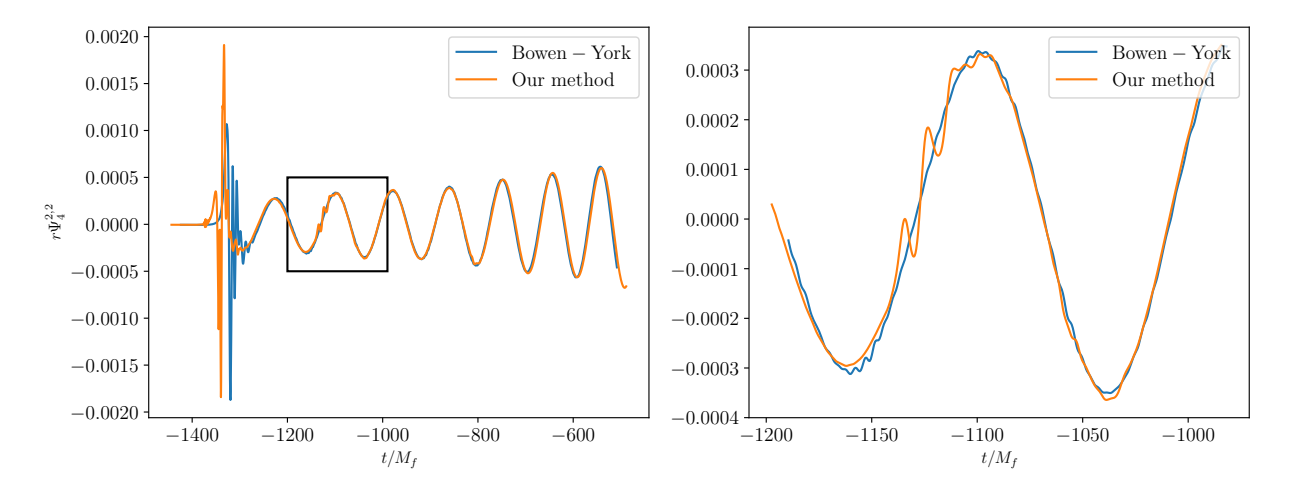


Figure 7: The gravitational radiation $r\Psi_4^{22}$ from the black hole inpiral of equalmass, with anti-aligned spin direction. The inner boundary condition for Ω is $\Omega|_{r=r_H}=\pm 82(3\cos^2\theta-1)$. The black holes have masses $M_1=M_2=0.5511$, spins $S_1=(0.1312,0,0),\ S_2=(-0.1312,0,0)$, and are initially placed at $x=\pm 6$. In the left panel, the enclosed box highlights an oscillatory pattern during the early phase of the merger. The right panel provides a zoomed-in view of this pattern.

We further examine the case $\Omega|_{r=r_H} = 80(5\cos^3\theta - 3\cos\theta)$, in which the angular velocity is prescribed with a more complex profile corresponding to the spherical harmonic component C_{30} (see the right panel in Fig. 3). Again, the waveform in Fig. 8 displays an oscillatory pattern reminiscent of those of ringdown signals.

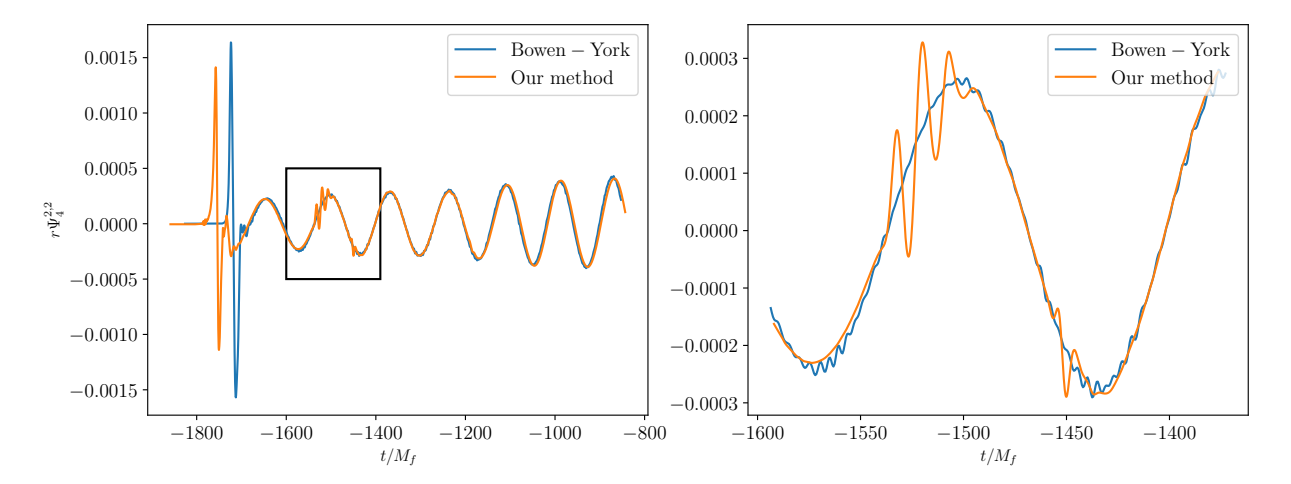


Figure 8: The gravitational radiation $r\Psi_4^{22}$ from the black hole inpiral of equalmass, with $\Omega|_{r=r_H} = 80(5\cos^3\theta - 3\cos\theta)$. The black holes have mass $M_1 = M_2 =$ 0.5160, spin $S_1 = S_2 = (10^{-8}, 0, 0)$, and are initially placed at $x = \pm 6$. In the left panel, the enclosed box highlights an oscillatory pattern during the early phase of the merger. The right panel provides a zoomed-in view of this pattern.

5. Concluding remarks

Based on a new geometric definition of the angular velocity of a rotating black hole, a new way to construct initial data for binary black holes is proposed. The new construction enables us to relate the geometry and dynamics at the horizon to the waveform at null infinity. The Hamiltonian and momentum constraints are formulated as a system of coupled elliptic equations for the conformal factor ψ and the angular velocity Ω , subject to appropriate boundary conditions at the horizons and at infinity.

Waveform simulations in the conformally flat case using the new data suggest that, during the inspiral phase of binary black hole coalescence, new features of the waveform appears. This holds the promise that, in the detection of gravitational waves in space when many orbital cycles in the inspiral phase of black hole coalescence is expected to be observed, we will see new waveforms distinct from those currently observed by LIGO detection. The present framework also allows the inclusion of matter in the constraint equations. The resulting initial data may then be used to probe the structure of neutron stars through their associated waveforms near null infinity. These problems remain to be studied in our future work.

Acknowledgements

This work is dedicated to Professor Ke Wu on the occasion of his 80th birthday, for his outstanding contributions to the development of mathematical physics in China. The computations were partly done on the high performance computers of State Key Laboratory of Scientific and Engineering Computing, Chinese Academy of Sciences.

The work was supported by the National Key Research and Development Program of China (Grant No. 2021YFC2202501). The authors also acknowledge support from the National Natural Science Foundation of China (Grant No. W2431012).

References

- [1] Xuefeng Feng, Ruodi Yan, Sijie Gao, Yun-Kau Lau, and Shing-Tung Yau. Geometric inequality for axisymmetric black holes with angular momentum. *Classical and Quantum Gravity*, 42(6):065022, 2025.
- [2] Reiner Kuhnau. Handbook of Complex Analysis. Elsevier, 2002.
- [3] Jeffrey M Bowen and James W York Jr. Time-asymmetric initial data for black holes and black-hole collisions. *Physical Review D*, 21(8):2047, 1980.
- [4] LORENE: Langage objet pour la relativité numérique. https://lorene.obspm.fr/.
- [5] Eric Gourgoulhon, Philippe Grandclement, Keisuke Taniguchi, Jean-Alain Marck, and Silvano Bonazzola. Quasiequilibrium sequences of synchronized and irrotational binary neutron stars in general relativity: Method and tests. *Physical Review D*, 63(6):064029, 2001.
- [6] Philippe Grandclément, Eric Gourgoulhon, and Silvano Bonazzola. Binary black holes in circular orbits. ii. numerical methods and first results. Physical Review D, 65(4):044021, 2002.
- [7] Frank Löffler, Joshua Faber, Eloisa Bentivegna, Tanja Bode, Peter Diener, Roland Haas, Ian Hinder, Bruno C Mundim, Christian D Ott, Erik Schnetter, et al. The einstein toolkit: a community computational infrastructure for relativistic astrophysics. Classical and Quantum Gravity, 29(11):115001, 2012.
- [8] Maxwell Rizzo, Roland Haas, Steven R. Brandt, Zachariah Etienne, Deborah Ferguson, Lucas Timotheo Sanches, Bing-Jyun Tsao, Leonardo Werneck, David Boyer, Gabriele Bozzola, et al. The Einstein Toolkit. The "Martin D. Kruskal" release, ET_2025_05. doi:10.5281/zenodo.15520463.
- [9] Marcus Ansorg, Bernd Brügmann, and Wolfgang Tichy. A single-domain spectral method for black hole puncture data. *Phys. Rev. D*, 70:064011, 2004.
- [10] J. David Brown, Peter Diener, Olivier Sarbach, Erik Schnetter, and Manuel Tiglio. Turduckening black holes: an analytical and computational study. *Phys. Rev. D*, 79:044023, 2009.
- [11] McLachlan, a public BSSN code. https://www.cct.lsu.edu/~eschnett/McLachlan/.
- [12] Masaru Shibata and Takashi Nakamura. Evolution of three-dimensional gravitational waves: Harmonic slicing case. *Physical Review D*, 52(10):5428, 1995.
- [13] Thomas W Baumgarte and Stuart L Shapiro. Numerical integration of einstein's field equations. Physical Review D, 59(2):024007, 1998.
- [14] Erik Schnetter, Scott H. Hawley, and Ian Hawke. Evolutions in 3-D numerical relativity using fixed mesh refinement. Class. Quantum Grav., 21:1465–1488, 2004.
- [15] Jonathan Thornburg. A Fast Apparent-Horizon Finder for 3-Dimensional Cartesian Grids in Numerical Relativity. Class. Quantum Grav., 21:743–766, 2004.
- [16] Olaf Dreyer, Badri Krishnan, Deirdre Shoemaker, and Erik Schnetter. Introduction to isolated horizons in numerical relativity. *Phys. Rev. D*, 67:024018, 2003.
- [17] Demetrios Christodoulou. Reversible and irreversible transformations in black-hole physics. *Physical Review Letters*, 25(22):1596, 1970.
- [18] J David Brown and James W York Jr. Quasilocal energy and conserved charges derived from the gravitational action. *Physical Review D*, 47(4):1407, 1993.
- [19] Abhay Ashtekar, Christopher Beetle, and Jerzy Lewandowski. Mechanics of rotating isolated horizons. *Physical Review D*, 64(4):044016, 2001.
- [20] Abhay Ashtekar and Badri Krishnan. Dynamical horizons and their properties. *Physical Review* D, 68(10):104030, 2003.

- [21] Sergio Dain, Carlos O Lousto, and Ryoji Takahashi. New conformally flat initial data for spinning black holes. *Physical Review D*, 65(10):104038, 2002.
- [22] Geoffrey Lovelace, Robert Owen, Harald P Pfeiffer, and Tony Chu. Binary-black-hole initial data with nearly extremal spins. *Physical Review D*, 78(8):084017, 2008.
- [23] Yeong-Bok Bae, Young-Hwan Hyun, and Gungwon Kang. Ringdown gravitational waves from close scattering of two black holes. *Physical Review Letters*, 132(26):261401, 2024.